Direct FEM computation of turbulent multiphase flow in 3D priting nozzle design

Ezhilmathi Krishnasamy[a,b,*], Johan Jansson[a,b]

[a] *Department of Electrical Engineering and Computer Science, KTH Royal Institute of Technology, Sweden*
[b] *Basque Center of Applied Mathematics, Bilbao, Spain*

Abstract

In this paper, we present a nozzle design of the 3D printing using FEniCS-HPC as mathematical and simulation tool. In recent years 3D printing or Additive Manufacturing (AM) has become a emerging technology and it has been already in use for many industries. 3D printing considered as a sustainable production or eco-friendly production, where one can minimize the wastage of the material during the production. Many industries are replacing their traditional parts or product manufacturing into optimized or smart 3D printing technology. In order to have 3D printing to be efficient, this should have optimized nozzle design. Here we design the nozzle for the titanium material. Since it is a metal during the process it has to be preserved by the inert gas. All this makes this problem comes under the multiphase flow. FEniCS-HPC is high level mathematical tool, where one can easily modify a mathematical equations according to the physics and has a good scalability on massively super computer architecture. And this problem modelled as Direct FEM/General Galerkin methodology for turbulent incompressible variable-density flow in FEniCS-HPC.

Keywords: Direct FEM, Multiphase flow, Variable density, Turbulence, 3D printing and FEniCS-HPC

*Corresponding author
Email addresses: kriezh@kth.se (Ezhilmathi Krishnasamy), jjan@kth.se (Johan Jansson)

1. Introduction

The overall goal of the FRACTAL project led by Etxe-Tar is to design a 3D printing nozzle for a selective laser melting method, where a fiber laser will be used as an energy source to melt an inter gas and powder mixture jet ejected by the nozzle. Where the entire metal melting process is confined by the inert gas (argon) to ensure minimizing oxygen interaction and hydrogen pick up. 3D printing, also know as additive manufacturing (AM) has gained popularity in recent years, especially in the medicine industries, where to make orthopedic components such as knee, hip, jaw replacements[1, 2]; and also it uses increases in consumer products and mechanical industries. For example, General Electronics (GE) produces a 3D printing spare parts for it's next generation LEAP jet engines[3]. And in medicine (bio-mechanical), each and every patient has a unique structure, to replace their body parts in a quick way 3D printing is a good option. It is estimated that, to produce knee implant component with traditional method produces up to 80% metal waste chips[4].

In order to design efficient 3D printing nozzle, we have conducted 3 stages of research for the nozzle, they are:

- Initial design
- Optimized design
- Compare the simulation results with experimental results

A efficient 3D printing nozzle should have this properties, which are as follows:

1. Minimize a wastage of the titanium powder (titanium is expensive)
2. Avoid oxidation during a melting process (might decrease the melting efficiency, nitrogen and oxygen pickup)
3. Minimize heating of tip of a nozzle (during the melting temperature might rise around 1,668 °C)

We consider a continuum multiphase model of the three phases, they are:

- Inert gas ans particle mixture
- Inert gas
- Air

In the presented simulations we omit the air phase for simplicity, but the model has the capability for including this third phase without significant extra complexity.The model is discretized by the Direct FEM Simulation (DFS) methodology in the FEniCS-HPC framework, and the simulations are carried out on the Beskow supercomputer.

2. Mathematical model

We model the problem by the primitive incompressible Navier-Stokes equations with variable density ρ:

$$\begin{aligned} R(\hat{u}) &= \begin{cases} \rho(\partial_t u + (u \cdot \nabla)u) + \nabla p - \nu \Delta u - \rho g = 0 \\ \partial_t \rho + (u \cdot \nabla)\rho = 0 \\ \nabla \cdot u = 0 \end{cases} \\ \hat{u} &= (u, p, \rho) \end{aligned}$$

The different phases are then simply modeled by different boundary values for the density ρ. We here consider a constant dynamic viscosity ν, and zero gravity g. The unknowns are the velocity u, density ρ and pressure p. An inflow boundary condition is set for the velocity u, and an outflow conditionn $p = 0$ for the pressure.

By using our adaptive finite element method (AFEM) we are not introducing any explicit parametrization in the discretization, meaning that we can control the computational error. We do however introduce a modeling error in terms of the slip boundary condition and in terms of the continuum model of the inter gas and particle mixture. We aim to validate the model against experiments together with Etxe-Tar.

2.1. Skin friction model

In our work on high Reynolds number turbulent flow [5, 6, 7, 8, 9], we have developed a skin friction wall layer model. That is, we append the NSE with the following boundary conditions:

$$u \cdot n = 0, \tag{1}$$

$$\beta u \cdot \tau_k + n^T \sigma \tau_k = 0, \quad k = 1, 2, \tag{2}$$

for $(x, t) \in \Gamma_{solid} \times I$, with $n = n(x)$ an outward unit normal vector, and $\tau_k = \tau_k(x)$ orthogonal unit tangent vectors of the solid boundary Γ_{solid}. We use matrix notation with all vectors v being column vectors and the corresponding row vector is denoted v^T.

For the present simulations we use the approximation $\beta = 0$ to allow cheap computation, meaning that we don't need to resolve high gradients in the boundary layer, which lead to high numerical dissipation if unresolved. We have previosuly shown that this model can be a good approximation for high Reynolds number, but likely introduces a modeling error for the more intermediate and low Reynolds numbers in the present setting. We aim to study the effect of varying the friction parameter during the course of the project.

2.2. The cG(1)cG(1) method for variable-density

In the DFS methodology, the mesh is adaptively constructed based on *a posteriori* estimation of the error in chosen goal or target functionals, such as drag and lift forces for example. Using duality in a variational framework, *a posteriori* error estimates can be derived in terms of the residual, the mesh size, and the solution of a "dual" (or "adjoint") problem [10]. We initiate the adaptive mesh refinement algorithm from a coarse mesh, fine enough to capture the geometry, but without any further assumptions on the solution.

This methodology is validated for a number of standard benchmark problems in the literature [11, 12, 13, 14], and in the following presentation we describe the

basic elements of DFS, also referred to as Adaptive DNS/LES, or G2 General Galerkin.

In a cG(1)cG(1) method [15] we seek an approximate space-time solution $\hat{U} = (D, U, P)$ (with D the discrete density ρ) which is continuous piecewise linear in space and time (equivalent to the implicit Crank-Nicolson method). With I a time interval with subintervals $I_n = (t_{n-1}, t_n)$, W^n a standard spatial finite element space of continuous piecewise linear functions, and W_0^n the functions in W^n which are zero on the boundary Γ, the cG(1)cG(1) method for variable-density incompressible flow with homogeneous Dirichlet boundary conditions for the velocity takes the form: for $n = 1, ..., N$, find $(D^n U^n, P^n) \equiv (D(t_n), U(t_n), P(t_n))$ with $D^n \in W^n$, $U^n \in V_0^n \equiv [W_0^n]^3$ and $P^n \in W^n$, such that

$$\begin{aligned} r(\hat{U}, \hat{v}) &= (D((U^n - U^{n-1})k_n^{-1} + (\bar{U}^n \cdot \nabla)\bar{U}^n), v) + (2\nu\epsilon(\bar{U}^n), \epsilon(v)) \\ &- (P, \nabla \cdot v) - (Dg, v) + (\nabla \cdot \bar{U}^n, q) + (D^n - D^{n-1})k_n^{-1} + (\bar{U}^n \cdot \nabla)\bar{D}^n), v) \\ &+ LS(D, U, P) + SC(D, U, P) = 0, \ \forall \hat{v} = (z, v, q) \in W^n \times V_0^n \times W^n \end{aligned} \quad (3)$$

where $\bar{U}^n = 1/2(U^n + U^{n-1})$ is piecewise constant in time over I_n and LS and SC are least-squares and shock-capturing stabilizing term described in [15].

2.3. The FEniCS-HPC finite element computational framework

The simulations in this report have been computed using the Unicorn solver in the FEniCS-HPC automated FEM software framework.

FEniCS-HPC is an open source framework for automated solution of PDE on massively parallel architectures, providing automated evaluation of variational forms given a high-level description in mathematical notation, duality-based adaptive error control, implicit parameter-free turbulence modeling by use of stabilized FEM and strong linear scaling up to thousands of cores [16, 17, 18, 19, 20, 21]. FEniCS-HPC is a branch of the FEniCS [22, 23] framework focusing on high performance on massively parallel architectures.

Unicorn is solver technology (models, methods, algorithms and software) with the goal of automated high performance simulation of realistic continuum

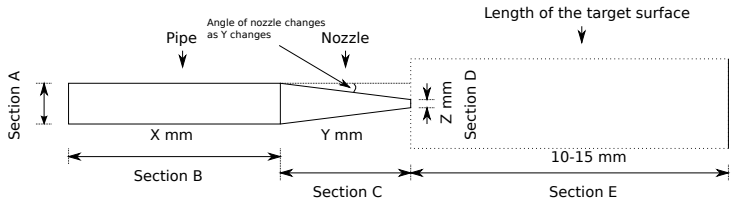

Figure 1: Schematic 3D printing nozzle design.

mechanics applications, such as drag or lift computation for fixed or flexible objects (FSI) in turbulent incompressible or compressible flow. The basis for Unicorn is Unified Continuum (UC) modeling [24] formulated in Euler (laboratory) coordinates, together with the General Galerkin (G2) adaptive stabilized finite element discretization described above.

3. Design Phase

3.1. Initial Design

First we would like to see how the jet of flow will be look like in reality and how far it can be steady before it breaks, to do this we have come up with simple cone shape model. Figure 1 shows the initial design of the 3D printing prototype. FEniCS-HPC does not have adaptivity for the multiphase flow, in this case, we ran couple of adaptive simulation for one-phase flow and we took that mesh as a initial mesh for the multiphase flow, for example this mesh can be seen in Figure 5. During the design phase the following items should be considered, they are, laster beam diameter is 150 µm and distance from a nozzle tip to the target surface should be between 10 mm to 15 mm

Figure 2 and 3 show a multiphase flow with velocities profiles and different section of cone size. As we can see in here, higher velocity seems to be stable compare to the lower velocity.

3.2. Optimized design

In this design phase we introduce a sheath flow [25], which will make the flow steady and narrow down a jet flow, this concept of geometry can seen in

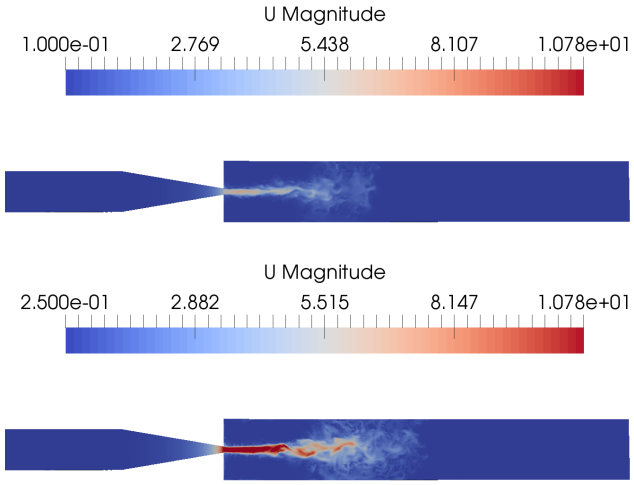

Figure 2: Nozzle length (section c)is 2.5mm and velocities ={0.1, 0.25} m/s

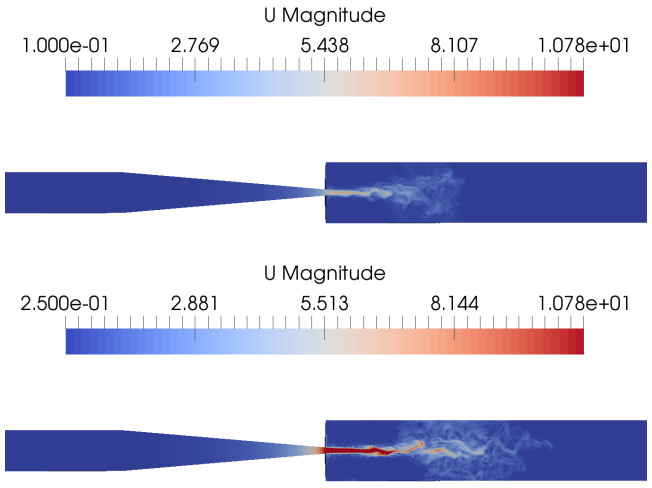

Figure 3: Nozzle length (section c)is 5.0mm and velocities ={0.1, 0.25} m/s

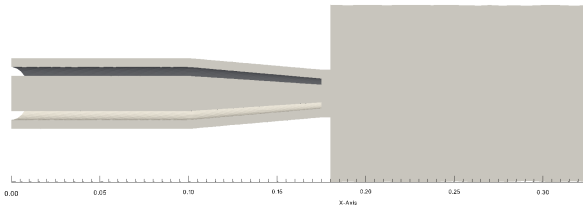

Figure 4: Schematic 3D printing sheath model

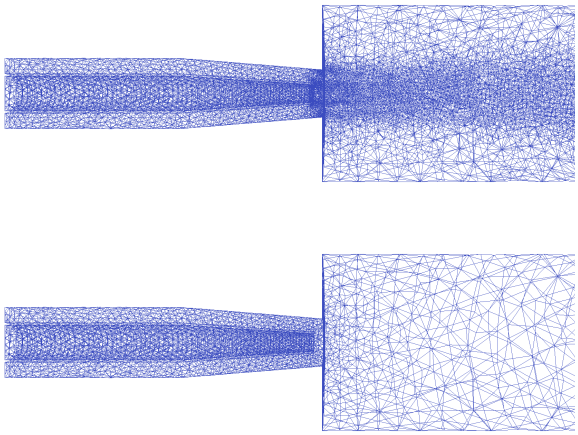

Figure 5: Adaptivity mesh for the single phase flow

Figure 4. Sheath flow has a real benefit which can be seen in the figures 6 and 7

3.3. Validation

In this stage we got experimental results 3D printing nozzle, which is almost similar to the sheath modeling which we discussed above. Figure 8 shows the design of the model and reference sample points location.

4. Results

The equation (2) can be scaled arbitrarily keeping the Reynolds number fixed, using the formula for the Reynolds number $Re = \frac{\rho \bar{u} L}{\nu}$ with $\bar{u}$ the freestream velocity, L the characteristic length and ν the viscosity.

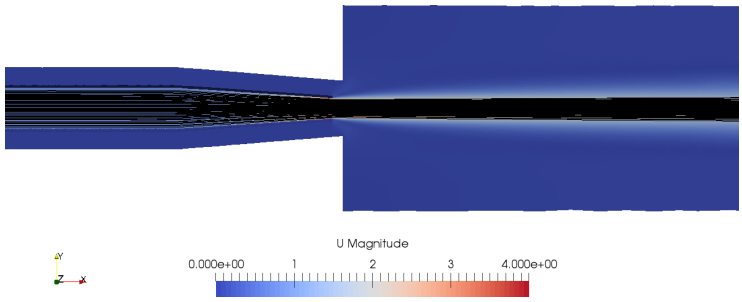

Figure 6: Schematic 3D printing sheath model

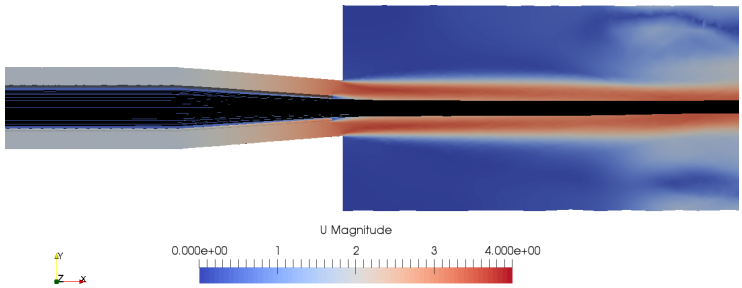

Figure 7: Adaptivity mesh for the single phase flow

In the presented simulations we choose the physical geometrical dimensions, where L can be chosen as the diameter of the inner channel, $L = 0.8mm$. We choose $\rho_{mixture} = 1$, and $\rho_{inert} = 1e-3$. The inner inflow is chosen as $u_{inner} = 0.75$. We then study a range of sheath inflow velocities and viscosities to study the different flow regimes, and the focusing effect of the sheath flow.

We give a schematic of plot lines in figure 8, used for studying the density distribution in subsequent plots. The density field in a slice through the center of the domain is given in figures 9, 10, 11 for a range of sheath inflow speeds indicated in the plots. In figures 12, 13, and 14 the density along the specified plot lines.

We use the same mesh for all the simulations, which has been constructed by adaptive one-phase simulations, where we make the coarse approximation that the velocity field for one-phase flow will be similar to the multi-phase case in the present simulations.

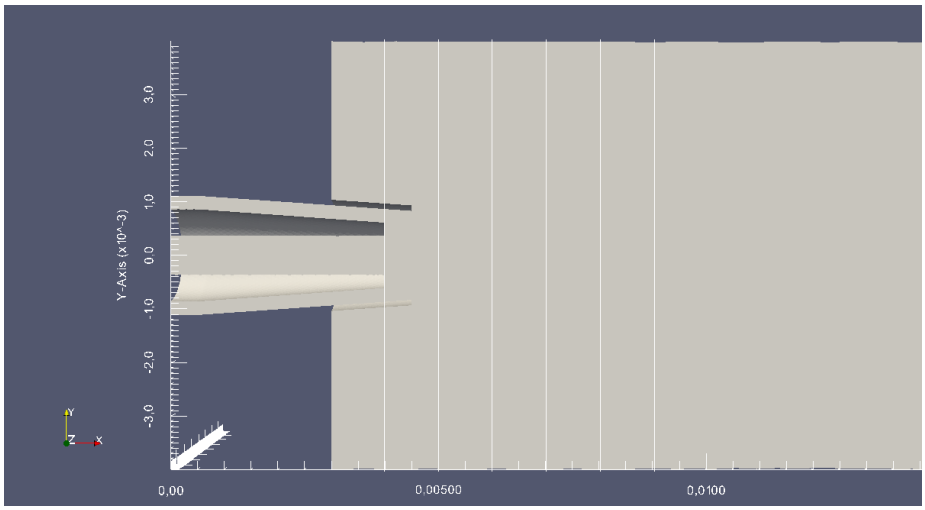

Figure 8: Plot line positions = 0.0, 1.0, 2.0, 3.0, 4.0 and 5.0 mm

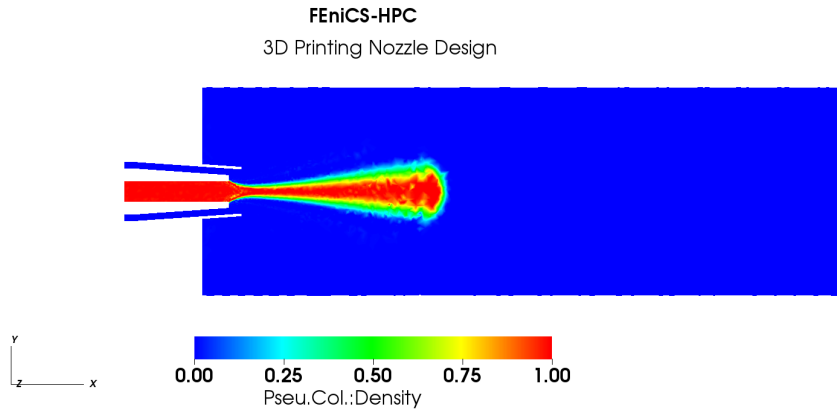

Figure 9: Pseu.Col.:Density; viscosity ν = 1e-04, inner inflow $u_{inner} = 0.75$ and sheath inflow $u_{sheath} = 3.75$.

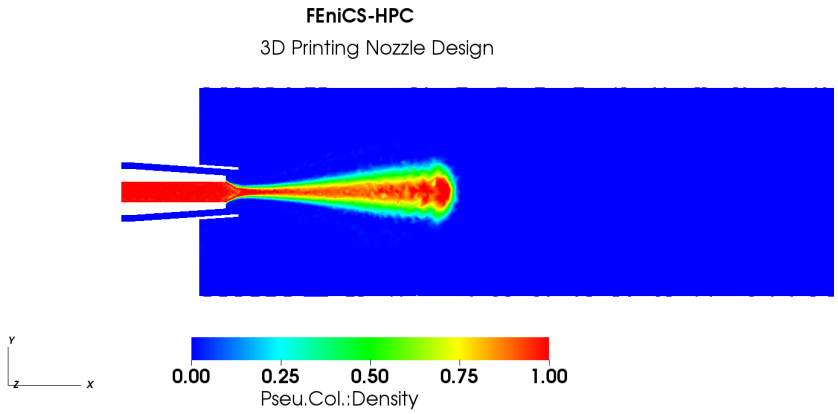

Figure 10: Pseu.Col.:Density; viscosity ν = 1e-04, inner inflow $u_{inner} = 0.75$ and sheath inflow $u_{sheath} = 4.75$.

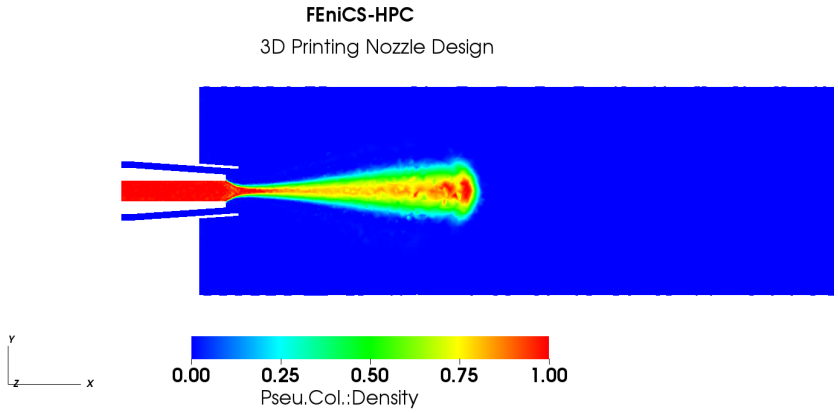

Figure 11: Pseu.Col.:Density; viscosity ν = 1e-04, inner inflow $u_{inner} = 0.75$ and sheath inflow $u_{sheath} = 5.75$.

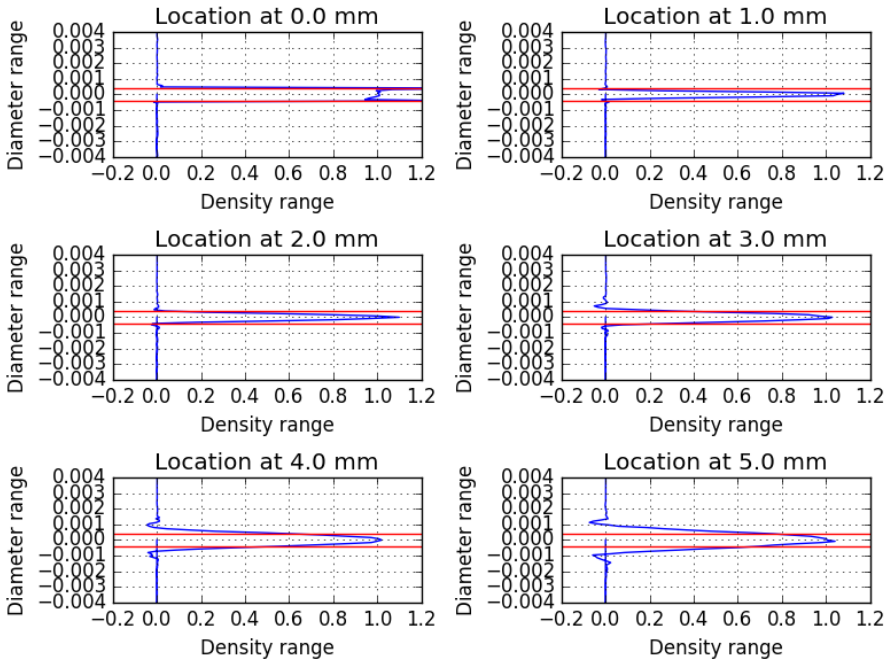

Figure 12: viscosity ν = 1e-04, inner inflow $u_{inner} = 0.75$ and sheath inflow $u_{sheath} = 3.75$.

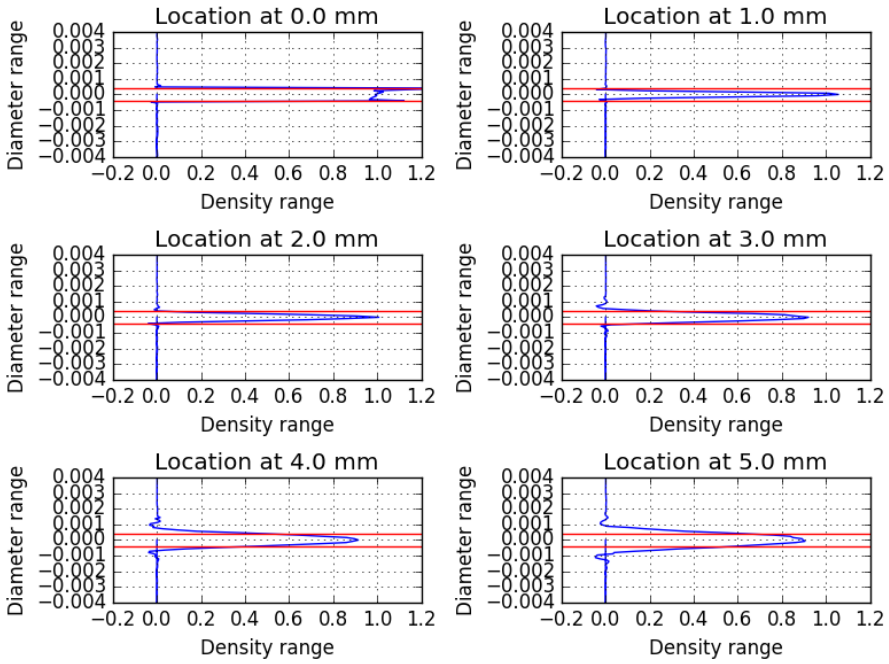

Figure 13: viscosity ν = 1e-04, inner inflow $u_{inner} = 0.75$ and sheath inflow $u_{sheath} = 4.75$.

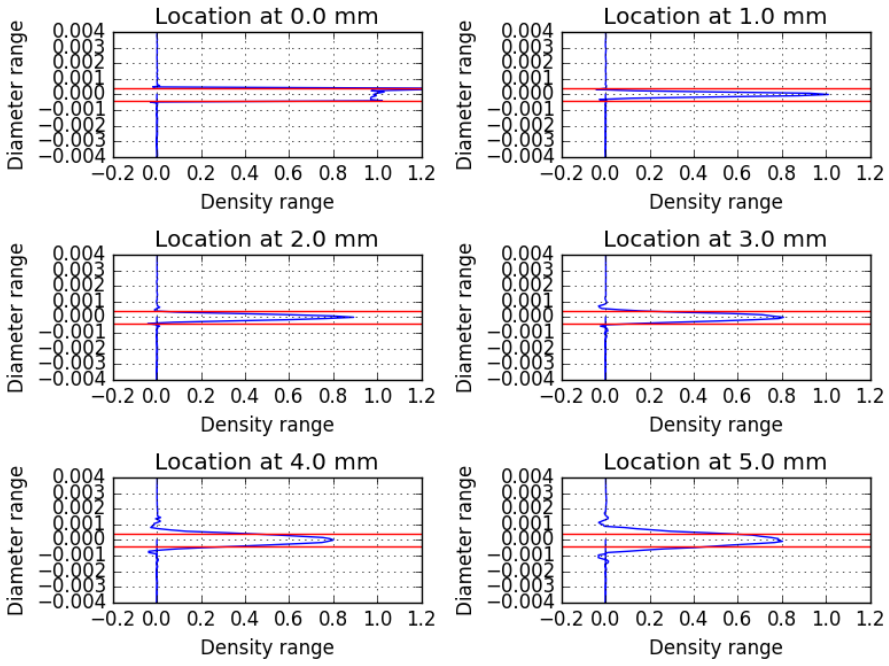

Figure 14: viscosity ν = 1e-04, inner inflow $u_{inner} = 0.75$ and sheath inflow $u_{sheath} = 5.75$.

5. Summary and Conclusion

From our simulation results we see that the dominant parameter, aside from the viscosity, is the sheath velocity. The geometry of the nozzle appears to have less importance. We have thus focused on studying the sheath inflow speed in this report.

In the figures 12, 13, and 14 we see that as the speed of the sheath flow is increased, the width of the inert gas and particle mixture jet is decreased. The parameters corresponding to 14 appear to give the best results among the studied cases.

Some outstanding questions are:

- Are we able to reproduce the flow regime seen in the simulations in the laboratory experiments?

- How large is the modeling error from the continuum assumption in the mathematical model?

Acknowledgment

We would like to thank BCAM for the financial support and Exte-Tar for the experimental results. And also we would like to thank the PDC/KTH Sweden for the computational resource.

References

[1] J. W. Choi, N. Kim, Clinical application of three-dimensional printing technology in craniofacial plastic surgery, Archives of plastic surgery 42 (3) (2015) 267–277.

[2] S. L. Sing, J. An, W. Y. Yeong, F. E. Wiria, Laser and electron-beam powder-bed additive manufacturing of metallic implants: A review on processes, materials and designs, Journal of Orthopaedic Research.

[3] S. C. Joshi, A. A. Sheikh, 3d printing in aerospace and its long-term sustainability, Virtual and Physical Prototyping (2015) 1–11.

[4] L. Murr, S. Quinones, S. Gaytan, M. Lopez, A. Rodela, E. Martinez, D. Hernandez, E. Martinez, F. Medina, R. Wicker, Microstructure and mechanical behavior of ti–6al–4v produced by rapid-layer manufacturing, for biomedical applications, Journal of the mechanical behavior of biomedical materials 2 (1) (2009) 20–32.

[5] J. Hoffman, N. Jansson, A computational study of turbulent flow separation for a circular cylinder using skin friction boundary conditions, Ercoftac, series Vol.16, Springer, 2010.

[6] J. Hoffman, C. Johnson, Resolution of d'alembert's paradox, J. Math. Fluid Mech.

[7] R. Vilela de Abreu, N. Jansson, J. Hoffman, Adaptive computation of aeroacoustic sources for a rudimentary landing gear, Int. J. Numer. Meth. Fluids 74 (6) (2014) 406–421. doi:doi:10.1002/fld.3856.
URL http://dx.doi.org/10.1002/fld.3856

[8] J. Hoffman, J. Jansson, C. Johnson, New theory of flight, Journal of Mathematical Fluid Mechanics.

[9] J. Hoffman, J. Jansson, N. Jansson, R. V. D. Abreu, Towards a parameter-free method for high reynolds number turbulent flow simulation based on adaptive finite element approximation, Computer Methods in Applied Mechanics and Engineering 288 (0) (2015) 60 – 74, error Estimation and Adaptivity for Nonlinear and Time-Dependent Problems. doi:http://dx.doi.org/10.1016/j.cma.2014.12.004.
URL http://www.sciencedirect.com/science/article/pii/S0045782514004836

[10] J. Hoffman, C. Johnson, Computational Turbulent Incompressible Flow, Vol. 4 of Applied Mathematics: Body and Soul, Springer, 2007.

[11] J. Hoffman, Computation of mean drag for bluff body problems using adaptive dns/les, SIAM J. Sci. Comput. 27(1) (2005) 184–207.

[12] J. Hoffman, Adaptive simulation of the turbulent flow past a sphere, J. Fluid Mech. 568 (2006) 77–88.

[13] J. Hoffman, C. Johnson, A new approach to computational turbulence modeling, Comput. Methods Appl. Mech. Engrg. 195 (2006) 2865–2880.

[14] J. Hoffman, Efficient computation of mean drag for the subcritical flow past a circular cylinder using general galerkin g2, Int. J. Numer. Meth. Fluids 59(11) (2009) 1241–1258.

[15] J. Hoffman, C. Johnson, Computational Turbulent Incompressible Flow: Applied Mathematics Body and Soul Vol 4, Springer-Verlag Publishing, 2006.

[16] J. Hoffman, J. Jansson, R. V. de Abreu, N. C. Degirmenci, N. Jansson, K. Müller, M. Nazarov, J. H. Spühler, Unicorn: Parallel adaptive finite element simulation of turbulent flow and fluid-structure interaction for deforming domains and complex geometry, Computers and Fluids.

[17] J. Hoffman, J. Jansson, C. Degirmenci, N. Jansson, M. Nazarov, Unicorn: a Unified Continuum Mechanics Solver, Springer, 2012, Ch. 18.

[18] N. Jansson, J. Hoffman, J. Jansson, Framework for Massively Parallel Adaptive Finite Element Computational Fluid Dynamics on Tetrahedral Meshes, SIAM J. Sci. Comput. 34 (1) (2012) C24–C41.

[19] R. C. Kirby, FIAT: Numerical Construction of Finite Element Basis Functions,, Springer, 2012, Ch. 13.

[20] J. Hoffman, J. Jansson, N. Jansson, M. Nazarov, Unicorn: A unified continuum mechanics solver, in: Automated Solutions of Differential Equations by the Finite Element Method, Springer, 2011.
URL http://www.fenicsproject.org/pub/documents/book/

[21] J. Hoffman, J. Jansson, N. Jansson, C. Johnson, R. V. de Abreu, Turbulent flow and fluid-structure interaction, in: Automated Solutions of Differential Equations by the Finite Element Method, Springer, 2011.
URL http://www.fenicsproject.org/pub/documents/book/

[22] A. Logg, K.-A. Mardal, G. N. Wells, et al., Automated Solution of Differential Equations by the Finite Element Method, Springer, 2012. doi:10.1007/978-3-642-23099-8.

[23] FEniCS, Fenics project, http://www.fenicsproject.org.

[24] J. Hoffman, J. Jansson, M. Stöckli, Unified continuum modeling of fluid-structure interaction, Mathematical Models and Methods in Applied Sciences.

[25] Y.-L. Pan, J. Bowersett, S. C. Hill, R. G. Pinnick, R. K. Chang, Noz-
240 zles for focusing aerosol particles, Tech. rep., ARMY RESEARCH LAB ADELPHI MD COMPUTATIONAL AND INFORMATION SCIENCES DIRECTORATE (2009).